Journal of Applied Electrochemistry (2007) 37:77–85
DOI 10.1007/s10800-006-9216-x

Effect of hydrodynamics on Faradaic current efficiency in a fluorine electrolyser

G. ESPINASSE[1], M. PEYRARD[2], F. NICOLAS[1] and J.P. CAIRE[3,*]
[1]*AREVA Business Unit Chimie, Secteur Mines Chimie Enrichissement, BP 16, 26701, Pierrelatte, France*
[2]*ASTEK Rhône Alpes, place du Verseau, 38130, Echirolles, France*
[3]*LEPMI, ENSEEG, UMR 5631 INPG – CNRS, 1130 Rue de la Piscine, 38402, Saint Martin d'Hères, France*
*(*author for correspondence, e-mail: Jean-Pierre.Caire@lepmi.inpg.fr)*

Received 14 February 2006; accepted in revised form 2 May 2006

Key words: current efficiency, electrolyser, fluorine, modelling, two-phase flow

Abstract

A fluid dynamics simulation was used to study the effect of the internal movement of hydrogen bubbles on current efficiency in a pilot scale fluorine electrolyser. Two dimensional modelling of the gas–liquid free convection was carried out using the Estet-Astrid (EA) finite volume code. The effect of hydrodynamics is well highlighted and calculations show that a significant fraction of the hydrogen bubbles can migrate, under certain conditions, into the fluorine compartment. This fraction of hydrogen recombines with fluorine and thus decreases the Faradaic current efficiency of the electrolyser. The numerical results confirm the experimental trends observed on the pilot. The model also clarifies the effect of hydrogen bubble diameter on Faradaic current efficiency.

1. Introduction

In any electrolyser, Faradaic current efficiency is a key parameter. Current efficiency is monitored in production because it is usually a good indicator of cell ageing. In most electrochemical processes, long-term studies and successive improvements have raised the current efficiency to values close to 100%. The few percents of current efficiency lost are usually explained by various causes (parasitic reactions, electric leaks), but also by a phenomenon which is seldom taken into account in models, the hydrodynamics of the cell. This study focuses on the effect of the hydrodynamics of the two-phase electrolyte on Faradaic current efficiency in the particular case of fluorine electrolysis.

Fluorine electrolysis [1–3] is particularly interesting because overpotentials are very large, thermal phenomena are significant [4, 5], fluorine emission is not conventional and free convection makes the temperature uniform in the cell [1]. The characteristics of fluorine bubble release are not yet completely understood and a specific study is in progress. In a fluorine electrolyser the couplings between charge, mass, thermal and momentum transfers are particularly strong. A digital model was gradually developed to take into account all these coupled phenomena [2, 6–9]. The final model uses the coupling of two commercial codes distributed by Astek [10], Flux-Expert (FE) and Estet-Astrid (EA).

The first code FE is based on the finite element method and is used to compute the charge and heat transfer in the cell. The CFD software EA is devoted to the modelling of two-phase flow and thermal transfer in the stirred electrolyte. EA is a software package developed by Electricité de France to simulate highly complex turbulent flows, especially two-phase flows containing dispersed inclusions such as bubbles, drops or particles. Here, an Eulerian two-phase approach is used. The structured meshing of the reactor was obtained from the Simail code. EA was chosen for its ability to handle the free convection of dispersed hydrogen bubbles in a dense molten salt electrolyte, to simulate the gas bubbles evolving at the electrodes and to be very stable in the thermal computation process as seen previously [1].

2. Pilot reactor

The test reactor is presented in Figure 1. Reactor operation was assumed to be steady state, though the computation of convection using EA is non-steady. In this scheme, at initial time, the electrolyte is assumed to be at rest and contains a null volume fraction of gas. The gas evolves at the electrodes and the plume begins to grow as the current is imposed.

3. Effect of hydrodynamics on current efficiency

As shown in Figure 1, there is no diaphragm but a simple skirt and a hydraulic safety valve to separate

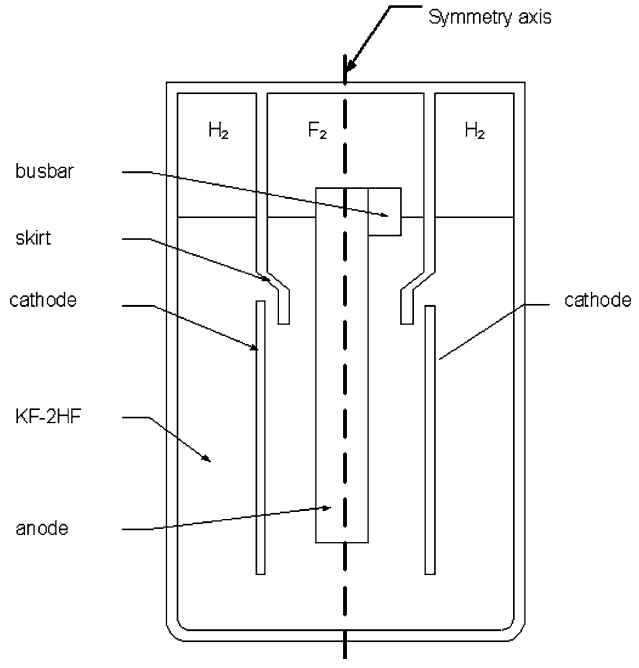

Fig. 1. 2D vertical cross section of the pilot reactor.

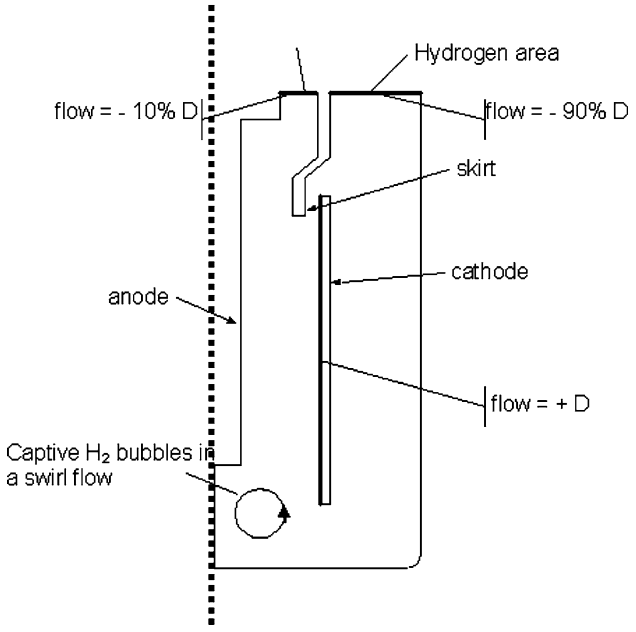

Fig. 2. A schematic example of hydrogen distribution leading to 90% current efficiency.

the two gas compartments in the fluorine electrolyser. The small, very light hydrogen bubbles evolving at the cathode are drawn along by the natural convection of the electrolyte. The skirt is placed between anode and cathode to divert the hydrogen bubbles towards the cathode compartment and away from the fluorine bubbles. It appears however that the finest bubbles of hydrogen are carried out by electrolyte swirls and are thus likely to migrate towards the anodic compartment. It is thought that any bubble of hydrogen passing into the fluorine compartment recombines instantaneously on contact with the curtain of fluorine bubbles slipping on the anode. This is particularly true for bubbles of very small diameter which are easily pulled by the liquid. Such small bubbles have a long residence time in the reactor, particularly when they are trapped in a swirl. Such a loss implies a drop in current efficiency. Figure 2 gives an example in which 10% of the produced hydrogen flow D would pass into the fluorine compartment leading to 90% current efficiency.

There is obviously no experimental way of visualizing the flow of the two-phase fluid, even in a simplified cell like that in Figure 1, because of the aggressiveness of the KF-2HF molten salt used in this electrolyser. Experiments carried out in the past on this pilot suggest that this recombination effect was far from negligible. Since numerical calculations can provide precise speed distributions for bubbles of a given diameter in such a reactor, it was interesting to check these assumptions. EA simulations presented here are aimed at estimating, for various bubble sizes and different current densities, the proportion of hydrogen likely to pass into the fluorine compartment and recombine.

4. Numerical model

Complete solution of the coupled equations for charge, mass, thermal and momentum transfer is excessively long and time consuming [1]. A single run in this case can take several days on a 4 Go bi Xeon workstation. To reduce computing times and to compare the Faradaic current efficiency of different configurations, the charge, mass and thermal transfer were not systematically calculated here. Current distributions and temperature fields were calculated and tabulated once before the runs to focus on the two-phase problem. This procedure is equivalent to a partial coupling of the different transfers. This assumption is justifiable because both the current distribution and the temperature fields are known to be almost homogeneous in this pilot. The temperature variations in the electrolyte are limited to a few degrees and undoubtedly contribute little to the hydrodynamics in comparison with the gas lift [1]. No other parasitic phenomena that might decrease current efficiency were taken into account in this study and the entire model was developed as a pure two-phase free convection problem using EA.

4.1. *Set of partial differential equations*

The free convection of the molten salt due to gas lift comes essentially from hydrogen evolving at the cathodes since the hydrogen bubbles adhere to the carbon and slip along the cathodes [1]. Since gas movement is essentially limited to a vertical cross section, the study can be restricted to a two-dimensional problem. Free convection is described by two mass transfer equations and two momentum equations written for each phase k ($k = 1$ for continuous phase and $k = 2$ for dispersed phase).

The momentum equation of phase k reads:

$$\alpha_k\rho_k\frac{\partial}{\partial t}U_{k,i}+\alpha_k\rho_k U_{k,j}\frac{\partial}{\partial x_j}U_{k,i}=-\alpha_k\frac{1}{\partial x_i}+\alpha_k\rho_k g_i\ +I_{k,i}-\Gamma_k U_{k,i}-\frac{\partial}{\partial x_j}\left[\alpha_k\rho_k\left\langle u'_{k,i}u'_{k,j}\right\rangle_k+\Theta_{k,ij}\right]. \quad (1)$$

The indices 1 and 2 are associated, respectively with the electrolyte and the hydrogen bubbles with the following notations:

α_k: Volume fraction of fluid k

$U_{k,i}$: ith component of the mean velocity for each phase k defined as:

$$U_{k,i}=\left\langle u_{k,i}\right\rangle_k \quad (2)$$

where $\langle\_\rangle_k$ is the mean operator and $u'_{k,i}$ the ith component of the fluctuating velocity for phase k defined as:

$$u_{k,i}=\left\langle u_{k,i}\right\rangle_k+u'_{k,i} \quad (3)$$

P_1: Pressure of the continuous phase (electrolyte)

g_i: ith component of gravity

$\langle u'_{1,i}\ u'_{1,j}\rangle_k$: Reynolds tensor for the liquid phase ($k = 1$)

$\langle u'_{2,i}\ u'_{2,j}\rangle_k$: Kinetic stress tensor for the gas phase ($k = 2$)

$\Theta_{1,ij}$: Molecular viscosity tensor for the liquid phase ($k = 1$).

The physical significance of the different terms of Equation (1) are:

$\alpha_k\rho_k\frac{\partial}{\partial t}U_{k,i}$ momentum variation

$\alpha_k\rho_k U_{k,j}\frac{\partial}{\partial x_j}U_{k,i}$ momentum transported by convection

$\alpha_k\frac{\partial P_1}{\partial x_i}$ momentum of pressure forces

$\alpha_k\rho_k\ g_i$ gravity force

$I_{k,i}$ interfacial momentum transferred between the two phases $\frac{\partial}{\partial_j}\left[\alpha_k\rho_k\left\langle u'_{k,i}u'_{k,j}\right\rangle_k+\Theta_{k,ij}\right]$ drag momentum

$\Gamma_k\ U_{k,i}$ mass transfer between the two phases.

The reciprocity of interaction implies:

$$I_{1,i}+I_{2,i}=0 \quad (4)$$

It is well known that the bubble size is not uniform in any electrolyser. Even if the bubbles generated by electrochemical are released with a uniform diameter, turbulence induces coalescence and breakage of bubbles [11] leading to a complicated distribution of bubble diameters which cannot be evaluated in a closed fluorine electrolyser. Hydrogen bubbles of various diameters are subjected to four main forces which influence their individual speed and trajectory, namely:

4.1.1. *Gravity*

$$F_1=\frac{\pi d^3\rho_g g}{6} \quad (5)$$

With:

d: bubble diameter (m)

g: gravitational acceleration (m s^{-2})

ρ_g: gas density (kg m^{-3})

ρ_l: liquid density (kg m^{-3})

4.1.2. *Buoyancy*

$$F_2=\frac{\pi d^3\rho_1 g}{6}. \quad (6)$$

4.1.3. *Force related to electrolyte flow*

The electrolyte flow exerts two forces on a bubble due to pressure and viscosity. Drag F_D is strongly related to the existence of the wake and is dominant for ill shaped particles, while lift or top spin F_P is most significant for well shaped particles, which is the case for a spherical gas bubble [11]. These forces are presented in Figure 3.

Drag is:

$$F_D=C_D\frac{\pi R^2\rho}{2}\left\|\overrightarrow{V^2}\right\|. \quad (7)$$

For spherical bubbles F_D is the mean drag coefficient given for a gas fraction $\alpha_2 < 0.2$ by:

$$F_D=\frac{3}{4}\frac{C_D}{\overline{d}}\left\langle\left|\overrightarrow{V_r}\right|\right\rangle_2 \quad (8)$$

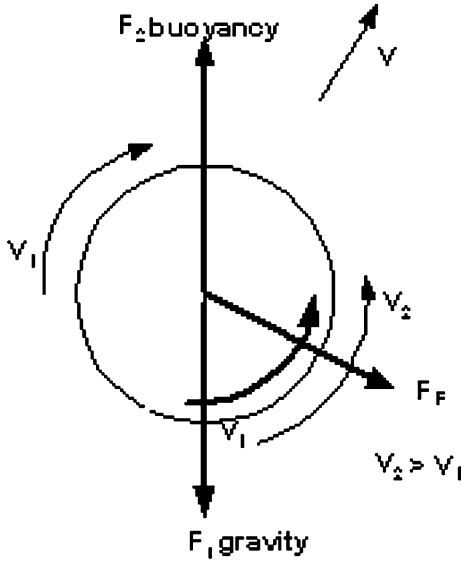

Fig. 3. Forces acting on a rotating gas bubble.

or the Ergun correlation [1] for $\alpha_2 > 0.2$:

$$F_D = \left[150\frac{\alpha_2}{Re} + 1,75\right]\frac{\left\langle\left|\overrightarrow{V_r}\right|\right\rangle_2}{\overline{d}} \quad (9)$$

Re is the mean bubble Reynolds dimensionless number:

$$Re = \frac{\alpha_1\left\langle\left|\overrightarrow{V_r}\right|\right\rangle_2\overline{d}}{v_1} \quad (10)$$

where ν_1 is the kinematic viscosity of the continuous phase and $\overline{d}$ the mean particle diameter: $\left\langle\left|\overrightarrow{V_r}\right|\right\rangle_2$ is the mean relative instantaneous velocity given by:

$$\left\langle\left|\overrightarrow{V_r}\right|\right\rangle_2 \cong V_{r,i}V_{r,i} + \left\langle v'_{r,i}v'_{r,i}\right\rangle_2 \quad (11)$$

with:

$$v_{r,i} = u_{2,i} - \widetilde{u}_{1,i} \quad (12)$$

$$V_{r,i} = \left\langle u_{2,i} - \widetilde{u}_{1,i}\right\rangle_2 \quad (13)$$

$$v_{r,i} = V_{r,i} + v'_{r,i} \quad (14)$$

$\widetilde{u}_{1,i}$ is the local fluid velocity not perturbed by the particle, i.e., the fluid velocity that could be measured at the centre in the absence of particles.

In Equation (7), C_D is the mean drag coefficient and is equal to 0.44 for $Re > 1000$ and defined for $Re < 1000$ by:

$$C_D = \frac{24}{Re}\left[1 + 0,15Re^{0,687}\right]\alpha_1^{-1,7} \quad (15)$$

Lift is:

$$F_L = 2\pi\rho_1 d^2\left\|\overrightarrow{V}^2\right\|C_L \quad (16)$$

where C_L is the lift coefficient.

4.1.4. *Added mass*

The force related to the particle acceleration that draws the fluid along is called added mass:

$$F_A = C_A\frac{2\pi\rho_1 d^3}{3}\frac{\partial V_i}{\partial x_i} \quad (17)$$

where C_A is the added mass coefficient equal to C_L [1].

It must be emphasized that the four forces all depend on bubble diameter d in a non-linear way. It should also be noted that the average drag coefficient F_D defined in Equations (7) and (8) tends towards the infinite when the bubble diameter d tends towards 0. Thus the trajectories of the hydrogen bubbles depend strongly on their diameter.

EA takes into account all the forces described in Equations (7–16). The free convection computation uses a Eulerian model with two equations ($k = 1$ for the continuous phase and $k = 2$ for the dispersed phase (hydrogen) [12].

We observed that both the drag and the added mass generated numerical instabilities for small bubble diameters. This is not surprising when we look at Equations (7) and (8) where d appears in the denominator. Then at very small bubble diameters, the bubbles are practically pulled by the liquid. The two-phase flow acts as a pure liquid and there is no need to take into account the relative motion of bubbles.

4.2. *Simulation process*

Although the reactor is assumed to function in steady state, computation of the free convection using EA is a non-steady process. In this scheme, at initial time, the electrolyte is assumed to be at rest and contains a null volume fraction of gas. The time iteration simulates plume spreading and numerical convergence is achieved when the plume of hydrogen bubbles is completely established.

The symmetry of the pilot was used to restrict the computations to a vertical cross section of half the reactor (see Figure 2). This assumption is correct in the absence of edge effects which could produce three dimensional convection in the electrolyser.

Simulation of the original fluorine bubbles has been described elsewhere [2]. Fluorine behaviour is much simpler to take into account since large fluorine bubbles adhere to the carbon, and slip along the vertical anode and are not likely to pass into the hydrogen compartment. While most of the hydrogen bubbles are normally evacuated into the proper compartment, a small proportion of gas is pulled towards the fluorine compartment by the free convection of the electrolyte. Figure 2 gives a schematic example where 10% of the hydrogen bubbles pass into the fluorine compartment, resulting in 90% current efficiency. This value does not take into account the bubbles that are captive in the swirls appearing in the reactor that are automatically taken into account by the EA computations. This effect could be studied in Lagrangian mode and the residence time distribution could be determined for different bubble diameters.

To compare and validate the digital simulations the calculated current efficiency values were compared with the measurements made on the test reactor presented in Figure 1.

4.3. *Physical data used in the study*

The dynamic viscosity μ of the electrolyte expressed in Pa s with temperature T in degrees K was [13, 14]

$$\mu = -1.194 \times 10^{-1} + 9.225 \times 10^{-4} \times T - 1.517 \times 10^{-6} \times T^2 \quad (18)$$

The dynamic viscosity of the electrolyte was calculated at 375 K, and the other data used for each phase are presented in Tables 1 and 2.

4.4. *Boundary conditions*

The boundary conditions presented in Figure 4 are standard, except for the anode where fluorine is released as a peculiar film [2]. This fluorine release is described here by a moving wall the speed of which was obtained previously from laser measurements in a small laboratory pilot [2]. Due to the large gap between anode and cathode, the current density was assumed to be uniform all along the cathode.

The hydrogen bubbles evolving at the cathode were modelled as a wall gas source calculated from the mean cell current. The code cannot take into account a diameter distribution of bubbles, and the hydrogen evolving at the cathode is converted into a flow of bubbles of single diameter which will form the plume. This assumption is not confirmed for a chlorate cell where the electrolyte is less dense and the bubbles are larger [15]. The flow and size of the hydrogen bubbles thus become the key parameters for the simulation.

For each run, the code is used to calculate the difference between the quantity of hydrogen generated at the cathode and the quantity actually produced, i.e., that which flows through the surface of the bath in the cathode compartment. The difference between the two terms represents the gas that is either circulated in the electrolyser or lost in the fluorine compartment. It is assumed that in both cases the fraction of electrochemically generated hydrogen lost by the two mechanisms recombines with fluorine and decreases the Faradaic current efficiency.

To model Faradaic yield, a possible exit for hydrogen is required in each compartment, as seen in Figure 4. A permeable interface situated at the two free gas/electrolyte interfaces was used as boundary condition for hydrogen (upper interface in Figure 4).

Table 1. Parameters used for the continuous phase (molten salt KF, 2HF)

Pressure	101300 Pa
Density (ρ)	1900 kg m^{-3}
Dynamic viscosity (ν)	5.936×10^{-6} m^2 s^{-1}

Table 2. Parameters used for the dispersed phase (hydrogen)

Density (ρ)	0.0667 kg m^{-3}
Dynamic viscosity (ν)	1.5×10^{-4} m^2 s^{-1}
Bubble diameter	0.0003–0.001 m

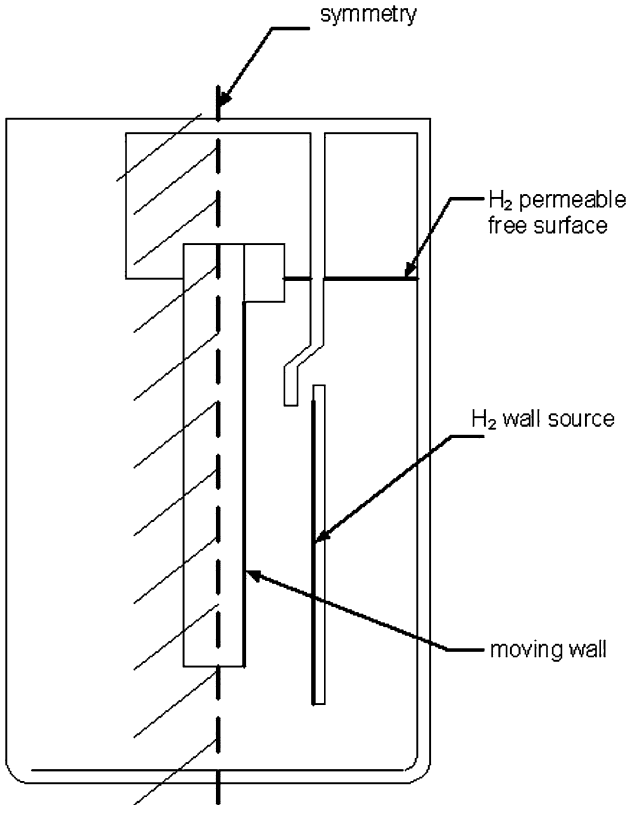

Fig. 4. Boundary conditions.

4.5. *Anode boundary conditions*

Although the bubbles of fluorine adhere to the carbon interface, they move upwards, and it is assumed that all the evolved fluorine escapes into the fluorine compartment. The drive effect exerted by the fluorine bubbles on the liquid molten salt observed by Roustan [2] is represented by a constant-speed moving wall boundary condition at the anode.

4.6. *Cathode boundary conditions*

To simulate the production of hydrogen bubbles, wall sources were imposed along the cathode. The previous electrokinetic study showed that the current density was appreciably uniform in the cell and it was thus assumed that hydrogen was released uniformly over the entire electrode height.

Theoretically, hydrogen bubbles detach from the wall without speed but they are immediately pulled by the fluid out of the hydraulic boundary layer. Because of the electrolyte movement and the relative movement of gas the hydrogen flow was directed at an angle of 45° from the electrode. The true experimental angle of detachment is not known but the first numerical tests have shown that the calculation does not converge without a value of this order of magnitude.

It was also assumed that the departure angle did not interfere with the various bubble diameters tested in this study. In fact, the release of hydrogen bubbles is probably much more complicated than the scheme suggests in this simplified model. However, this simple boundary condition has the merit of ensuring numerical convergence in good coherence with physical reality. The problem is thus primarily related to the hydrodynamics of hydrogen in the electrolyser and in particular to the fraction which passes into the fluorine compartment.

4.7. *Initial conditions*

Natural convection results from gaseous emission at the cathode and anode. At initial time, when the current is applied, it is assumed that the electrolyte contains no gas and that the pressure and velocity fields are null. These initial conditions act as if a constant current density was imposed at the initial time in the electrolyser with the electrolyte at rest. The situation is analogous to the starting of the real cell. The EA code then solves the equations simulating a time evolution and determines the pressure and velocity fields at each time step. Convergence is obtained when the fields are stable from one iteration to the next. Although the calculation time differs from the real one, with such boundary conditions, the iterative algorithm of the EA code gives a fair analogy for the starting of the real cell and helps visualize the time evolution of the hydrogen bubble plume. In contrast, the numerical search of the steady state inevitably represents a long-lasting computation.

4.8. *Algorithm and numerical method*

The finite volume method used by EA is widely described in the literature [1, 2, 12, 16]. The calculation domain, here the electrolyte of the cell, is meshed in elementary control volumes on which the mass and momentum assessments are carried out.

The mechanical equations of the fluids are discretized to be solved in each finite volume of the structured grid and so the code determines the velocity vectors, pressure and volume fraction at each node of the grid. Space discretization is dissociated from time discretization. A VF Quick-Upwind scheme with second order interpolation was used for space discretization and a usual finite differences scheme was used for time discretization [2, 12]. All these mathematical operations carried out on each finite control volume at each time step provide a discretized equation connecting each volume variable to its closest volumes. The set of discretized equations finally forms a matrix system which is numerically solved. To solve this non-linear system of equations at each time step, an iterative method is obviously required. Since the system is non-linear, each time step requires several iterative steps to solve the space coupling between velocity and pressure. A coupling speed–pressure algorithm of SIMPLE C type [17] was used in this study. The general idea of this algorithm is to correct the pressure and the velocity vectors at each iteration to ensure that they all verify the momentum and continuity equations at the same time.

4.9. *Computing time*

Transient iterative calculation is achieved when a steady or pseudo-steady state of velocity vectors is reached for both fluids. The evolution of the two components of the velocity vectors Vx, Vy is monitored during the calculation process thanks to numerical sensors judiciously placed in the electrolyte. During time iterations, the two components of the vectors initiated to zero evolve to reach an asymptote value which represents the steady state. The geometry considered here required approximately 200 s of real time to reach the steady state. It can be assumed that the real hydrodynamics of the pilot are stabilized in a few minutes. This steady state corresponds to the spreading of the hydrogen plume up to the free surface of the bath when the free convective movements are well established.

Bubble size obviously influences the hydrodynamics of the cell, as expected. While the bubble diameter distribution can easily be determined in these conditions, the results cannot be representative of the actual situation in the pilot where breakage and coalescence phenomena are quite different. But there are very few codes that can take into account such bubble distribution. Anta and al. [16] developed a software programme for this purpose and compared the plumes generated by different codes. They have shown that the distribution of bubble diameters has a real impact on the plume. It is therefore clear that the description of plumes made up of perfectly gauged bubbles is open to criticism [18–22].

Since EA only takes into account bubbles of uniform size we had to change the diameter of the bubbles at each run to estimate the effect of their diameter on the hydrodynamics. Table 3 shows that for each bubble size the time step had to be adjusted to ensure convergence. In this study it appeared that the iteration step varied on three decades when the bubble diameter was changed and that the computing times exploded when the size of the bubbles decreased.

5. Numerical results

5.1. *Gas distribution in the cell*

Figure 5 shows the distribution of the gas fraction in the cell obtained for a bubble size of 1 mm and for two current densities Io and 1.7 Io. This figure gives a fairly precise idea of the shape of the plumes of hydrogen bubbles when steady operation is reached. The figure shows that the stronger the current the larger is the plume of hydrogen bubbles spreading out at the top left of the cell. It appears that the skirt is only efficient at low current density since a significant part of the gaseous emission passes under the bus bar (at the left of the skirt) at high density. This fraction of the hydrogen bubbles that passes into the fluorine compartment reduces the current efficiency of the reactor.

Table 3. Computation durations for 200 s of real time using a biprocessor Intel Xeon 2.4 GHz workstation

	Time step	Computation time
Bubble diameter > 1 mm	0.01 s	5 h
Bubble diameter = 1 mm	0.001 s	12 h
Bubble diameter < 1 mm	0.0005 s	115 h

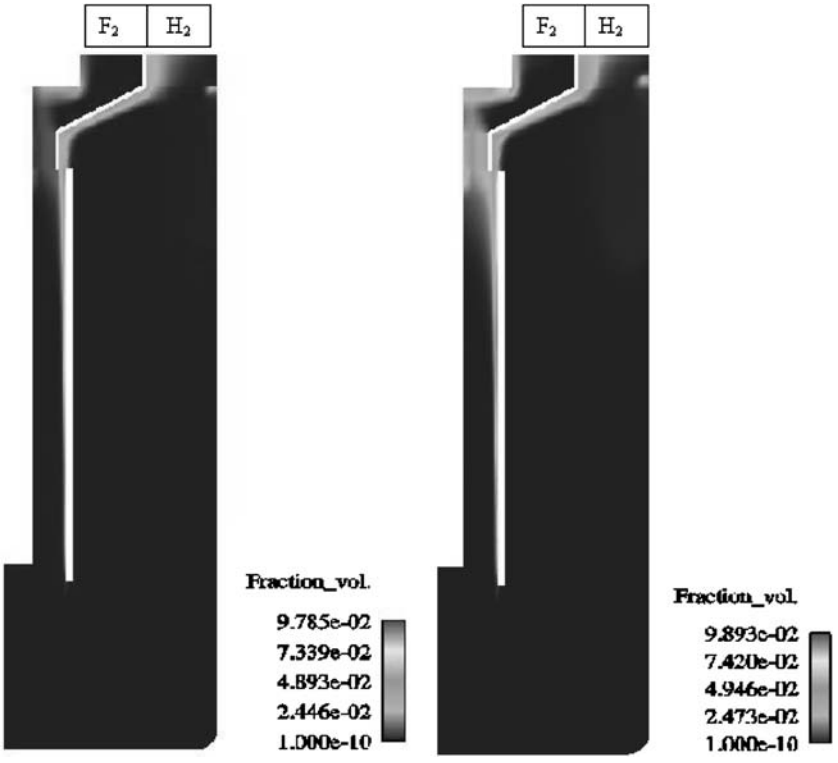

Fig. 5. Hydrogen mean gas fraction distribution for a given bubble diameter and two different current densities Io (left) and 1.7 Io (right).

5.2. *Variation in current efficiency with bubble diameter*

Current efficiency also decreases with the diameter of bubbles. This is not surprising when looking at Equations (1–20) since the four forces acting on bubble speed depend on the diameter in a non-linear way. Figure 6 shows the variation in current efficiency with the hydrogen bubble diameter for a cell current density Io. This result suggests that the fine bubbles are more easily pulled by the electrolyte convection. The plume then becomes larger and more bubbles can pass into the fluorine compartment.

By adjusting the bubble diameter the experimental curves observed were easily matched. The size obtained by calculation is in good agreement with the bubble dimensions observed visually in a laboratory micro pilot.

5.3. *Variation in Faradaic current efficiency with cell intensity*

The curves in Figure 7 calculated for two bubble diameters frame the experimental measurements pretty well after matching. This result is remarkable consider-

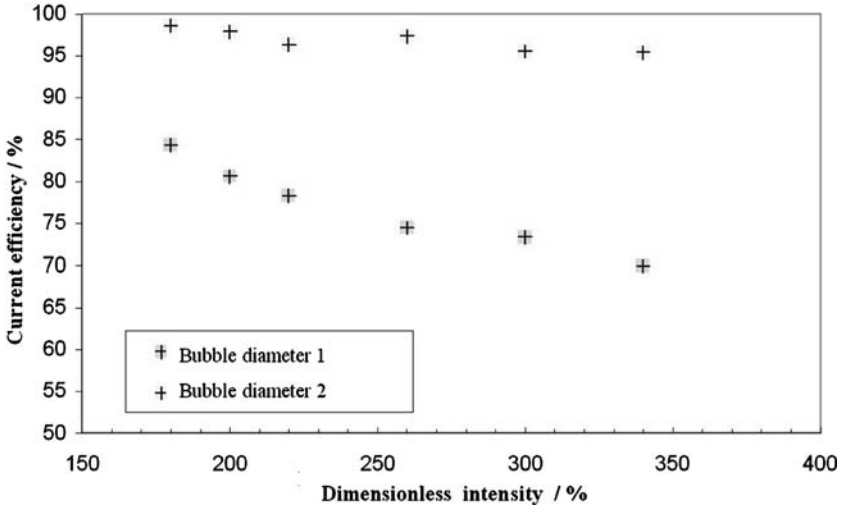

Fig. 6. Computed current efficiency vs. cell current intensity for a cathode–anode distance and two different diameters of bubbles.

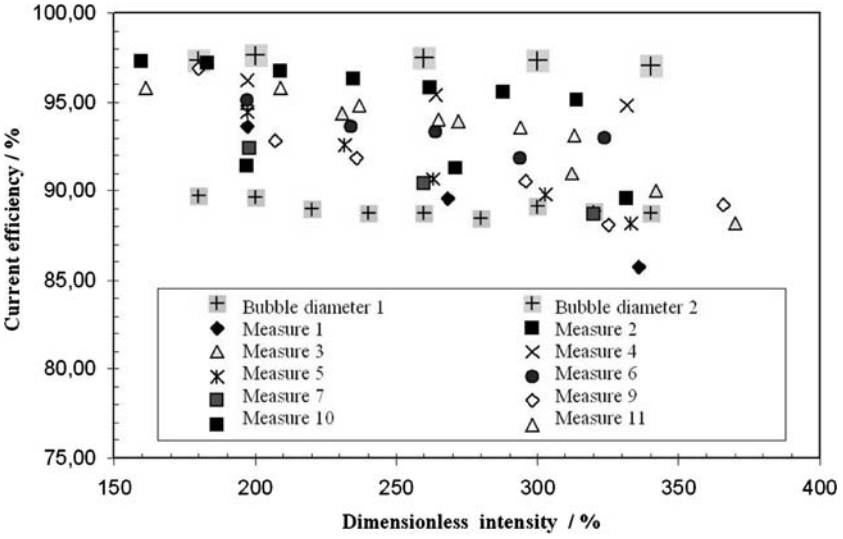

Fig. 7. Comparison of computed current efficiency for two different bubble diameters and measurements.

ing the assumption of a unique diameter of bubbles which is probably not very realistic. Figure 7 also shows that the simulation retrieves the decrease in current efficiency when the cell current increases. These results appear very satisfactory considering the assumptions made, the difficulty of measuring current efficiency in a fluorine cell and the underlying complexity of two-phase flows.

Eleven series of measurements made on the pilot were compared with the calculated variation in current efficiency in Figure 7. The agreement with experimental results is satisfactory and seems consistent considering the complexity of the computations and the assumptions made.

6. Conclusions

Hydrodynamics was found to have a real effect on current efficiency in the fluorine electrolyser. Calculations of two-phase flows using Estet-Astrid predicted the evolution of current efficiency according to current and the size of the hydrogen bubbles. As expected, a significant fraction of the evolved hydrogen is recirculated in the internal vortices and another fraction passes into the fluorine compartment. The model showed that the skirts placed to separate the gases are efficient at nominal current. At higher currents a significant fraction of the hydrogen bubbles passes into the fluorine compartment where they recombine, causing a drop in the total current efficiency of the electrolyser.

Due to the complexity of simulation, the calculations were limited to a vertical two dimensional cross section of the cell and hydrogen bubbles of single diameter. Nevertheless, the model explained the evolution of current efficiency observed on the pilot. The experimental current efficiency measured on the pilot could be matched by simple adjustment of hydrogen bubble diameter.

References

1. G. Espinasse, 'Modélisation d'un électrolyseur industriel de production de fluor par couplage des logiciels Flux-Expert & Estet-Astrid', (Mémoire de DRT, INPG, Grenoble, 2003).
2. H. Roustan, 'Modélisation des transferts couplés de charge et de chaleur dans un électrolyseur industriel de production de fluor', (INPG thesis, Grenoble, 1998).
3. H. Groult, D. Devilliers, F. Lantelme, J.P. Caire, M. Combel and F. Nicolas, *J. Electrochem. Soc.* **149** (2002) 485.
4. J.P. Caire, H. Roustan, F. Nicolas and P. Pham, Modélisation des transferts couplés de charges et de chaleur dans un électrolyseur à l'aide du logiciel Flux-Expert. *Entropie* **211** (1998) 47.
5. J.P. Caire, H. Roustan, F. Nicolas and P. Pham, Effect of fluid dynamics on thermal transfer in fluorine electrolyzer, AIDIC Conferences Series. Selected Papers of ECCE-1, RIS C.T. S.r.I. Milano, **2** (1997) 279.
6. H. Roustan, J.P. Caire, F. Nicolas and P. Pham, *J. Appl. Electrochem.* **28** (1998) 237.
7. H. Roustan, J.P. Caire, F. Nicolas and P. Pham, *in* J.W. Van Zee, T.F. Fuller, P.C. Foller and F. Hine (Eds), 'Advances in Mathematical Modeling and Simulation of Electrochemical Processes', *Electrochem. Soc. Proc. USA* **98-10** (1998) 202.
8. J.P. Caire, H. Roustan and F. Nicolas, 'Numerical Simulation of an Industrial Fluorine Electrolyzer',15th International Symposium on Fluorine Chemistry, The University of British Columbia, Vancouver, B.C., Canada, August 2–7, (1997).
9. H. Roustan, J.P. Caire, F. Nicolas and P. Pham, 'Thermal Modelling of an Industrial Fluorine Electrolyzer', Dechema, 15th International Symposium on Molten Salt Chemistry and Technology, Dresden, Germany, Proceedings, (1997) 0.60.1.
10. ASTEK SIMULOG, Equations et modèles diphasiques du Code ESTET-ASTRID (2001).
11. R. Clift, J.R. Grace and M.E. Weber, *Bubbles drops and particles* (Academic Press, New York, 1978).
12. SIMULOG, Présentation des équations de la mécanique des fluides. Manuel théorique du code ESTET-ASTRID version 3.5. Documentation utilisateur (2001).
13. I.A. Semerikova and A.N. Novikov, *Russian J. Phys. Chem.* **34**(11) (1960) 1216.
14. S.V. Patankar, *Numerical Heat Transfer and Fluid Flow, Series in Computational Methods in Mechanics and Thermal Sciences* (Hemisphere, Washington D.C., 1980).
15. R. Wetind, 'Two Phase Flows in Gas Evolving Electrochemical Applications', Thesis, KTH, Stockholm, (2001).
16. S.P. Antal, S.M. Ettorre, R.F. Kunz and M.Z. Podowski, *Development of a Next Generation Computer Code for the Prediction of*

Multicomponent Multiphase Flows, Proc. Int. Conf. on Multiphase Flow (ICMF, New Orleans, Los Angeles, 2001).
17. M. Blažej, G.M. Cartland Glover, S.C. Generalis and J. Markoš, *Chem. Eng. Proc.* **43** (2004) 137.
18. M.M. Vetyukov and A.F. Alabyshev, *Russian J. Phys. Chem.* **36**(5) (1962) 565.
19. S.V. Pantankar and D.B. Spalding, *Semi Implicit Method for Pressure Linked Equations, Numerical Heat Transfer and Fluid Flow* (McGrow-Hill, New York, 1980).
20. G.M. Cartland Glover and S.C. Generalis, *Chem. Eng. Proc.* **43** (2004) 101.
21. P.A. Solli, T. Eggen, E. Skybakmoen and A. Sterten, *J. Appl. Electrochem.* **27** (1997) 939.
22. A. Gobin, H. Neau, O. Simonin, J.R. Llinas, V. Reiling and J.L. Selo, *Int. J. Num. Meth. Fluids* **43** (2003) 1199.